

# A Computational Study of Bubble Formation from an Orifice Submerged in Liquid with Constant Gas Flow

James Q. Feng

OXCBO Research, Maple Grove, Minnesota, USA

[james.q.feng@gmail.com](mailto:james.q.feng@gmail.com)

## Abstract

The bubble formation process from an orifice submerged in liquid with constant gas flow is studied by numerical simulations using an OpenFOAM® volume-of-fluid solver. The computed results show that the detached bubble size tends to increase with the gas flow rate, orifice size, surface tension, liquid contact angle, etc. in qualitative agreement with most previous authors. For a given orifice size and liquid properties, there exists a critical gas flow rate above which detached bubbles will combine via coalescence known as bubble pairing. At low gas flow rates, the volume of detached bubbles in the quasi-static regime is shown to depend linearly on the gas flow rate, consistent with a physical mechanistic analysis but not recognized by previous authors. The detached bubble size seems insensitive to the contact angle when the liquid adequately wets the orifice wall but can increase substantially if the contact angle is increased beyond a critical value resulting in contact line motion on the horizontal outside wall of the orifice. The value of such a critical contact angle is found to increase with the orifice size and to decrease with the gas flow rate. Such revelations would logically suggest that reducing orifice size to generate smaller bubbles could be more challenging and practically difficult for sub-millimeter orifices with a constant gas flow.

**Keywords:** bubble formation, submerged orifice, constant gas flow, free surface, volume-of-fluid

## 1 Introduction

Flowing a gas through an upward-facing orifice into a liquid tank usually generates a sequence of bubbles, which has become essential in a wide range of phase contacting applications as seen in bubble columns, sparger reactors, extraction equipment, water treatment, etc. In terms of physics, a gas bubble grows with continuously flowing gas while attached along the contact line to the orifice wall before detaching, and freely rising in the liquid after the buoyancy force overcomes the capillary force. Yet the size of the detached bubble can be influenced by many factors such as gas flow rate, orifice size, wetting property of liquid on the orifice wall, and so forth, besides the balance of the buoyancy and surface tension. The bubble formation process often involves complicated fluid dynamics with free surface deformation,

disintegration, coalescence, and dynamic contact line motion. Its practical importance as well as theoretical modeling challenge has inspired numerous publications by generations of authors (cf. Harkins and Brown 1919; Clift et al. 1978; Gaddis and Vogelpohl 1986; Oguz and Prosperetti 1993; Ponter and Surati 1997; Kulkarni and Joshi 2005; Buwa et al. 2007; Ohta et al. 2011; Simmons et al. 2015).

Along with ample experimental results, theoretical models developed before 1980 were usually simplified based on force balances with spherically symmetric growing bubbles often assumed as a quasi-static process at a very low gas flow rate (as commented by Oguz and Prosperetti 1993; Buwa et al. 2007). To date, even with the available modern experimental equipment and numerical techniques, the general applicability of individually derived theoretical formulas remains elusive (Bari and Robinson, 2013). Due to the complexity of the dynamic process involved in bubble formation, an improved understanding of the fundamental physics may only be gained with more gap-filling model investigations and redundant comparisons as well as cross-examinations.

To simulate the mathematically difficult free-boundary fluid dynamics with minimal simplifying assumptions, various numerical methods for computational fluid dynamics (CFD) have been developed with the advent of powerful computers. For bubbles forming in inviscid or highly viscous liquids governed by linear field equations, a boundary-element (or boundary-integral) method (BEM) in terms of Green's functions with discretization only along the boundaries has been quite effective with results in apparent agreement with some experiments (e.g., Oguz and Prosperetti 1993; Wong et al. 1998; Higuera 2005). The restriction to linear field equations can be eliminated by solving the full nonlinear Navier-Stokes equations with a tessellation of the entire problem domain, which led to the development of several versions of arbitrary Lagrangian-Eulerian (ALE) methods capable of dealing with large deformations of boundary shapes governed by nonlinear field equations (e.g., Kistler and Scriven 1983; Christodoulou and Scriven 1992) as exemplified in computing highly deformed bubbles (Feng 2007) and bubble formation dynamics up to neck pinch-off (Simmons et al. 2015).

However, the difficulties in computing the situation with free surface disintegration and coalescence with the ALE methods have motivated developing the purely Eulerian methods such as volume of fluid (VOF by Hirt and Nichols 1981), level set method (LSM by Sussman et al. 1998), as well as coupled level set and volume of fluid (CLSVOF by Sussman and Puckett 2000), for effective simulations of bubble detaching dynamics (e.g, Krishna et al. 1999; Buwa et al. 2007; Nichita et al. 2010; Ohta et al. 2011; Sudeepta Vaishnavi et al. 2023). Unlike ALE with boundary-fitting moving meshes able to track free surface accurately, the resolution of free surface position in VOF simulations depends directly on the Eulerian mesh size; therefore, accurate free surface shape in VOF computation can usually be achieved at the expense of a much finer mesh than typical ALE meshes.

Although effective numerical methodologies appear well-established, most computational codes used in publications are not easily accessible. Code development from scratch even with the well-known methods can be very resource demanding, and almost prohibitive to most small organization researchers. Fortunately, several open-source software packages have been made available in recent years with computational capabilities comparable, sometimes even superior, to those popular commercial packages. Among others, the OpenFOAM® package consists of a

variety of commonly-used CFD solvers and boundary conditions, with powerful meshing utilities and postprocessing capabilities; it allows users to freely download the C++ source code for close examination and custom modifications, with a large user base across engineering and scientific communities for convenient exchanging knowledge. Hence, a recent version (v2206) of the OpenFOAM® VOF solver is selected for self-consistent simulations of the bubble formation process.

Besides providing a gap-filling model investigation, the present monograph with a systematic analysis of tabulated computational data for practically representative cases could also serve as benchmarks for future research comparison. In what follows, section 2 concisely describes the computational model setup, with computational results for a set of case studies presented in section 3. Finally, section 4 provides concluding remarks, highlighting the significant findings of the present work.

## 2 Computational Model Description

Considered here is a gas with a constant flow rate through an inlet tube connected to an orifice flowing into a liquid tank, as shown in figure 1a. The two-phase fluid flow problem is assumed axisymmetric, enabling the use of a wedge-type mesh (figure 1b) generated with the OpenFOAM® meshing utilities such as blockMesh, mergeMeshes, and stitchMesh for combining fine and coarse mesh patches to reduce computational burden while the free surface location can be adequately resolved (e.g., with the side length of local quadrilateral cells on the order of one-hundredth of the bubble diameter to ensure the variations of computed results within a few percent, as suggested by Ohta et al. 2011, Feng 2017, and further verified by the present mesh refinement tests.).

The chosen solver for this type of two-phase flow problem is named interIsoFoam—an improved VOF solver detailed by Roenby et al. (2016), Gamet et al. (2020), and reviewed by Mulbah et al. (2022) as a scheme for high accuracy at low computational cost. Because the description of this type of VOF solver is available in published literature (cf. Feng 2017, among others), it is unnecessary to repeat the details here (cf. Feng 2017 among others), it is unnecessary to repeat the details here. Briefly in simple terms, the VOF method treats the fluid interface as the “jump” of a scalar phase fraction field from 0 to 1, located in those cells containing fraction values (other than 0 and 1) in an Eulerian mesh. Movements of the scalar phase fraction are governed by a transport equation describing the advection of it with the flow. Then, the traction boundary condition at the free interface is transformed into a body force term associated with the gradient of the scalar phase fraction field in the Navier-Stokes momentum equations in an Eulerian frame, eliminating the need to deal with a moving mesh. It especially makes the simulations of bubble-detaching dynamics much less challenging.

In the present model, the nominal values for liquid phase density and dynamic viscosity are  $\rho = 1000 \text{ kg m}^{-3}$  and  $\mu = 0.001 \text{ kg m}^{-1} \text{ s}^{-1}$  (i.e., 1 cp), whereas those corresponding to the gas phase are  $1.2 \text{ kg m}^{-3}$  and  $1.8 \times 10^{-5} \text{ kg m}^{-1} \text{ s}^{-1}$  (0.018 cp), respectively specified for the VOF computations. Over orders-of-magnitude contrasts between liquid and gas phases in terms of these corresponding values would make the influence of gas-phase density and viscosity on the general fluid dynamical behavior almost irrelevant; therefore, only the liquid density and

viscosity are considered in the analysis and discussion. The surface tension value at the gas-liquid interface is taken as  $\sigma = 0.07 \text{ kg s}^{-2}$ , closely representing the air-water situation.

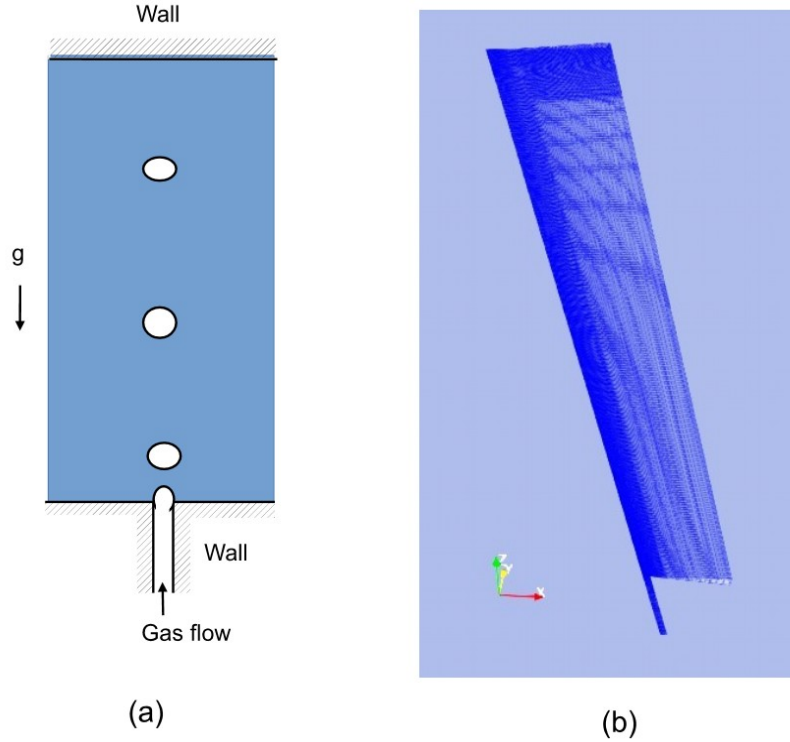


Figure 1. (a) Schematic of bubble formation when a gas flows through an orifice into a liquid tank; (b) A wedge mesh (discretized into quadrilateral finite-volume cells in two-dimensional space) with a combination of fine and coarse mesh patches, used for simulations of the axisymmetric two-phase flows in the present bubble formation problem

To complete the case specification, the boundary conditions used at the gas inlet are the uniform fixed value type for the velocity vector  $U = (0, 0, U_z)$  with  $U_z = \text{constant}$  and zeroGradient for the piezometric pressure  $p$  (cf. description in Feng 2017), at solid walls the noSlip type for  $U$  and zeroGradient for  $p$ , at the open lateral boundary a pressureInletOutletVelocity condition for  $U$  and a fixed value type for  $p$  (e.g.,  $= 10^5 \text{ Pa}$ ). At the gas-liquid-solid three-phase contact line, the available dynamicAlphaContactAngle condition is applied as is by specifying the static contact angle  $\theta_0$ , advancing contact angle  $\theta_A$ , and receding contact angle  $\theta_R$  as well as a  $u_\theta$  value. Here, for a specified static contact angle  $\theta_0$  the advancing contact angle and receding contact angle are always assigned as  $\theta_A = \theta_0 + 15^\circ$  and  $\theta_R = \theta_0 - 15^\circ$  with a fixed value of  $u_\theta$  (i.e.,  $= 1 \text{ m s}^{-1}$ ) to keep the presentation logically streamlined and self-consistent. Without losing generality, computed cases in the present work would have a nominal

contact angle  $\theta_0 = 45^\circ$  (corresponding to a partially wetting liquid at the solid wall) unless otherwise specified.

Per OpenFOAM<sup>®</sup> solver development requirements, each solver must come with at least one tutorial case. In fact, many popular solvers could have multiple tutorial cases provided with the standard downloadable packages. This can be very convenient for users who would not want to spend much time deciphering the exact meanings of those numerical scheme parameters; some of the tutorial parameter settings can indeed be directly used for similar computational problems without the need for modifications. For example, the numerical scheme parameters used in the present work for fvScheme and fvSolution are directly copied from the interIsoFoam tutorial case of “damBreak”, using the typical “Euler” implicit time scheme for temporal integration with adjustable time step under the restriction of Courant number  $< 0.2$ .

### 3 Results and Discussion

Before computing numerical solutions, it is heuristic to estimate a few reference parameters often used in the literature (e.g., Oguz and Prosperetti 1993; Ohta et al. 2011; Simmons et al. 2015). According to a static force balance between surface tension and buoyancy (Fritz 1935; van Krevelen and Hoftijzer 1950; Kumar and Kuloor 1970), the Fritz bubble volume  $V_F$  and corresponding bubble diameter  $d_F$  may be estimated with simple equations,

$$\sigma \pi d_c = \rho g V_F = \frac{\rho g \pi d_F^3}{6}, \text{ thus } V_F = \frac{\sigma \pi d_c}{\rho g} \text{ and } d_F = \left( \frac{6 \sigma d_c}{\rho g} \right)^{1/3}, \quad (1)$$

where  $\rho$  denotes the mass density of the liquid,  $\sigma$  surface tension of the gas-liquid interface,  $g$  the acceleration of gravity, and  $d_c$  the diameter of the three-phase contact line at the orifice wall (which is often assumed to be the same as the orifice diameter  $D$ .)

The analysis of Oguz and Prosperetti (1993) suggested that the Fritz volume and diameter can be only reasonable for the quasi-static situation when the gas flow rate  $Q \ll Q_{crit}$  where the critical gas flow rate may be expressed as

$$Q_{crit} = \pi \left( \frac{16}{3g^2} \right)^{1/6} \left( \frac{\sigma D}{2\rho} \right)^{5/6}. \quad (2)$$

At high gas flow rates, i.e.,  $Q > Q_{crit}$ , the bubbles would detach with a volume proportional to  $Q^{6/5}$ .

In this section, the nominal air-water system is examined first, with cases of variations in liquid viscosity and surface tension in subsequent subsections.

### 3.1 Air bubbles in water

For air bubbles in water with  $\rho = 1000 \text{ kg m}^{-3}$ ,  $\sigma = 0.07 \text{ kg s}^{-2}$ ,  $g = 9.81 \text{ m s}^{-2}$ , and  $\mu = 0.001 \text{ kg m}^{-1} \text{ s}^{-1}$  the value of the Ohnesorge number,

$$Oh = \frac{\mu g^{1/4}}{\rho^{1/4} \sigma^{3/4}}, \quad (3)$$

becomes  $2.313 \times 10^{-3}$ , suggesting that the liquid viscosity effect in an air-water system is negligible and an inviscid fluid model for bubble formation can yield reasonable results in agreement with experiments (as shown by Oguz and Prosperetti 1993).

An interesting special situation is that of  $d_F = d_c$  which yields

$$d_F = d_c = \sqrt{6} \times \sqrt{\frac{\sigma}{\rho g}} = 2.45 \times L_\sigma = 6.54 \times 10^{-3} \text{ m (or 6.54 mm)}, \quad (4)$$

where  $L_\sigma = \sqrt{\sigma/(\rho g)} = 2.67 \text{ mm}$  is regarded as the capillary scaling length (cf. Longuet-Higgins et al. 1991; Bari and Robinson 2013; Simmons et al. 2015). In other words, the bubble diameter in water is expected to be about the same as the contact line diameter at the orifice edge, when the orifice diameter  $D \sim 6.54 \text{ mm}$ . One of the cases presented by Oguz and Prosperetti (1993) with computed data and images of transient bubble shapes is that with  $D = 4 \text{ mm}$ , which is not too far from that given in (4) and could serve as a reference for comparison.

#### 3.1.1 Case of $D = 4 \text{ mm}$

For orifice diameter  $D = 4 \text{ mm}$ , the reference values of  $V_F$  and  $d_F$  are  $89.67 \text{ } \mu\text{L}$  (or  $\text{mm}^3$ ) and  $5.55 \text{ mm}$  with  $Q_{crit} = 3768.77 \text{ } \mu\text{L/s}$  (assuming  $d_c = D$ ) Figure 2 shows the computed results visualized with ParaView for bubble formation dynamics at various gas flow rates. As indicated by the spacing between the sequential bubbles, the bubble volume increases with the gas flow rate because the spacing does not decrease inversely proportional to the gas flow rate. For low gas flow rates  $Q < Q_{crit}$ , the detached bubbles rise following one another in a so-called period-1 regime with the bubble volume gradually increasing with  $Q$  (as shown in table 1). When  $Q \sim Q_{crit}$  (i.e., at  $U = 300 \text{ mm/s}$ ), the spacing between bubbles becomes so close that the coalescence of two neighboring bubbles occurs, resulting in pairing bubbles in the period-2 regime (cf. Buwa et al. 2007). Further increasing the gas flow rate would eventually lead to chaos via period-doubling (cf. Tufaile and Sartorelli 2000).

To provide more quantitative information, computed data of bubble detachment period  $\Delta T$  with the corresponding bubble volume  $V$  (derived from  $V = \Delta T \times Q$  which matches the numerical integration result along the free surface of the detached bubbles) and diameter  $d$  are given in table 1, with a reference to the  $Q / Q_{crit}$  value for  $D = 4 \text{ mm}$ . In comparison with the results by Oguz and Prosperetti (1993) for  $Q = 0.008$  and  $0.016 \text{ } \mu\text{L/s}$  as  $d = 5.188$  and  $5.277 \text{ mm}$ , the present results of  $d = 4.71$  and  $4.81 \text{ mm}$  are consistently smaller (by about 10%).

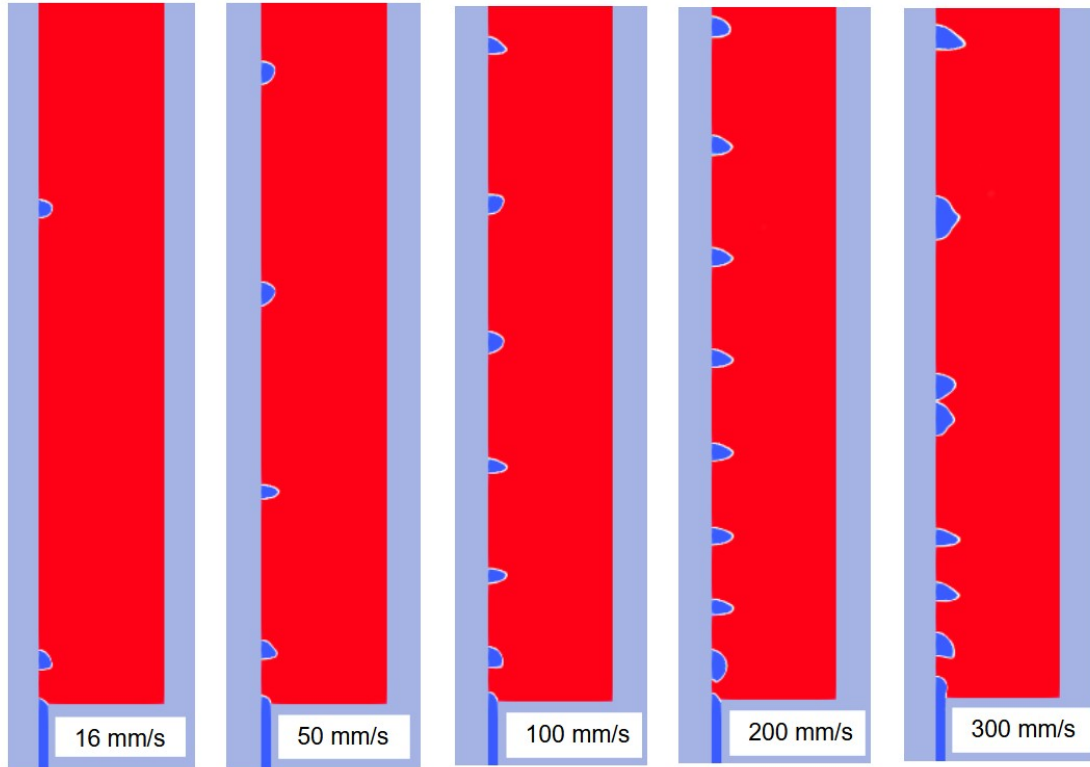


Figure 2. Formation of air bubbles in water from an orifice of diameter  $D = 4$  mm at various air-flow velocities (i.e.  $U = 0.016, 0.05, 0.1, 0.2, 0.3$  m/s corresponding to flow rate  $Q = 201, 628, 1257, 2513, 3770$   $\mu\text{L/s}$ ), simulated with the OpenFOAM<sup>®</sup> VOF solver interIsoFoam and visualized with the postprocessor ParaView.

Despite the numerical differences between those values and that of Oguz and Prosperetti (1993), we agree on the general trend of bubble size decreasing with reducing  $Q$ . Both of our values of  $V$  and  $d$  are less than the corresponding  $V_F (= 89.67 \mu\text{L})$  and  $d_F (= 5.55 \text{ mm})$  from (1) which are often regarded as the minimum values of bubble volume and diameter at the limit of so-called quasi-static bubble formation (at  $Q \ll Q_{crit}$ ). The fact that  $V_F$  and  $d_F$  can be inaccurate in quasi-static treatment was explained theoretically with the dynamic process of necking and pinch-off by Simmons et al. (2015) in a model with a pinned contact line. The need for correction to the Fritz volume  $V_F$  was also realized in an early publication by Harkins and Brown (1919).

More experimental evidence for  $V < V_F$  mostly with  $Q / Q_{crit} < 0.1$  has also been shown in the publications of Corchero et al. (2006), Bari and Robinson (2013), and Manoharan et al. (2021). According to the fitted power law of Bari and Robinson (2013) for measured quasi-static bubble volume  $V_B$  in experiments with fixed contact lines

$$\frac{V_B}{V_F} = 0.6863 \left( \frac{D}{L_\sigma} \right)^{-0.116}, \quad (5)$$

the value of  $V_B$  would become  $\sim 54.49 \text{ mm}^3$  for  $D = 4 \text{ mm}$  (with the capillary length in (4)  $L_\sigma = 2.67 \text{ mm}$ ), in agreement with the value of  $V$  in table 1 for  $Q \ll Q_{crit}$ .

Table 1. Computational results of air bubble detachment period  $\Delta T$ , corresponding bubble volume  $V$  and bubble diameter  $d$  with the value of  $Q / Q_{crit}$  for  $D = 4 \text{ mm}$  (at  $\theta_0 = 45^\circ$ )

$U$ (m/s)	$Q$ ( $\mu\text{L/s}$ )	$\Delta T$ (ms)	$V$ ( $\text{mm}^3$ )	$d$ (mm)	$Q / Q_{crit}$
0.008	100.5	545	54.79	4.71	0.0266
0.016	201.1	289	58.11	4.81	0.0533
0.05	628.3	113	71.00	5.14	0.167
0.1	1256.6	68	85.45	5.46	0.333
0.2	2513.3	50	125.66	6.21	0.667
0.3	3769.9	41	154.57	6.66	1.000

If the data in table 1 is plotted in terms of  $V$  versus  $x = Q / Q_{crit} (< 1)$ , a fitted line can be obtained as  $V(x) = 103.84 x + 52.71 \text{ mm}^3$  with  $R^2 > 0.997$ . Thus, the present results suggest a monotonic increase of  $V$  with  $Q$  and  $V(0) = 52.71 \text{ mm}^3$ , unlike what has been claimed by most other authors as the static regime wherein  $V$  becomes nearly constant for  $Q / Q_{crit} \ll 1$ . According to the data in table 1, the bubble size may become close to those of the Fritz value (1) in the  $Q / Q_{crit}$  interval between 0.1 and 0.5. The deviation of  $V$  from  $V(0)$  would be  $< 10\%$  for  $Q / Q_{crit} < 0.05$ .

The transient bubble free-surface profiles are shown in figure 3 during the bubble detachment process at  $U = 0.008, 0.016, 0.1 \text{ m/s}$ . A series of bubble surface profiles for  $U \sim 0.016 \text{ m/s}$  ( $Q \sim 200 \mu\text{L/s}$ ) were presented by Oguz and Prosperetti (1993), qualitatively comparable to the corresponding profiles in figure 3. However, an obvious discrepancy exists between their free surface shapes and those in figure 4 during attached bubble growth at particular time points, especially for  $t < -10 \text{ ms}$ . A closer examination reveals an inconsistency in their reported numerical free surface shapes which were intended for comparison with the experimental images by Longuet-Higgins et al. (1991) for about one bubble per second, likely with  $Q < 60 \mu\text{L/s}$  rather than  $\Delta T \sim 300 \text{ ms}$  with  $Q \sim 200 \mu\text{L/s}$ . Figure 4 shows that a well-developed neck appears at the free surface typically when  $t > -10 \text{ ms}$ , thereafter the time that takes for neck pinch-off would be almost independent of air flow rate but controlled by the capillary timescale (cf. Oguz and Prosperetti 1993),

$$t_\sigma = \sqrt{\frac{\rho D^3}{8\sigma}}, \quad (6)$$



which becomes 10.69 ms for  $D = 4$  mm (with  $\rho = 1000$  kg m<sup>3</sup> and  $\sigma = 0.07$  kg s<sup>-2</sup>).

Considering the physical mechanisms, the bubble formation process may be divided into two stages (cf. Clift et al. 1978; Simmons et al. 2015): the initial growth governed by the hydrostatic and capillary pressures, followed by a capillary-force driven dynamic event with considerable local velocity during necking and pinch-off. The timescale for the initial growth is expected according to the gas flow rate, namely proportional to  $V_F / Q$ , while that governing the necking dynamics is likely related to the capillary timescale  $t_\sigma$  in (6). At a low gas flow rate with the quasi-static bubble formation process, necking starts before the bubble volume reaches the static force-balance value  $V_F$  at a time  $\phi_b V_F / Q < V_F / Q$  until the bubble detachment, with a timescale  $\phi_a t_\sigma$  independent of  $Q$ , as evidenced in Fig. 4. When  $\Delta T = (\phi_a t_\sigma) + (\phi_b V_F / Q) < (V_F / Q)$ , the detached bubble volume,

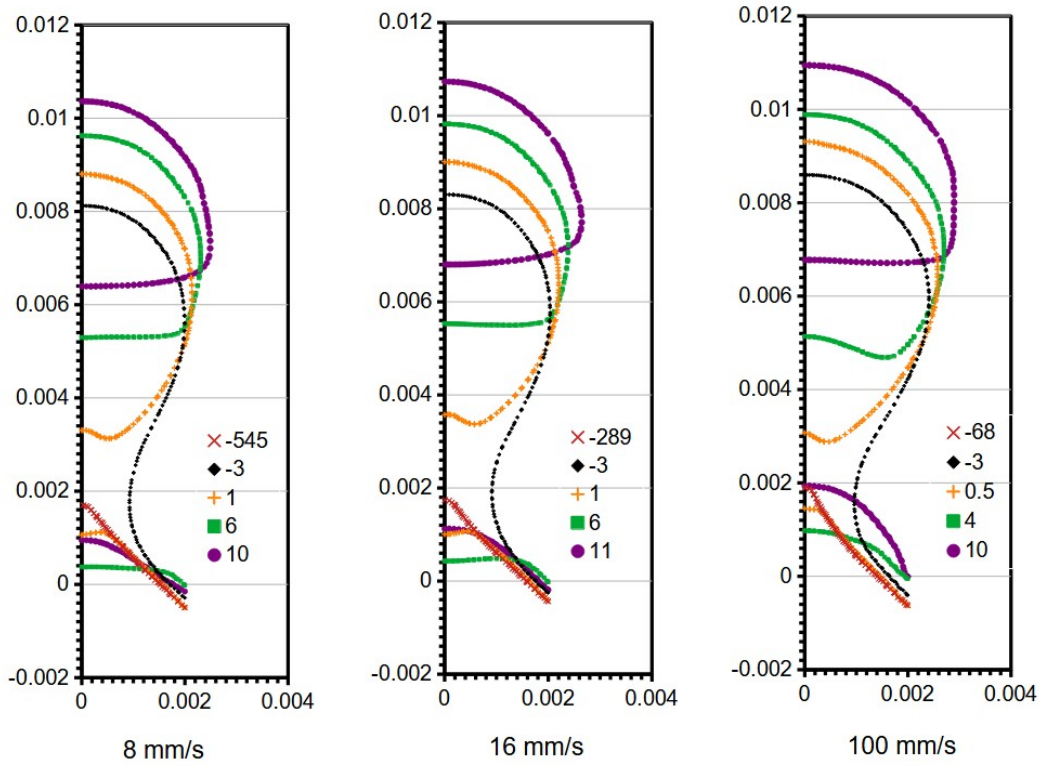


Figure 3. Free surface shapes during air bubble formation from an orifice of diameter  $D = 4$  mm in water at  $U = 0.008, 0.016, 0.1$  m/s corresponding to  $Q = 100.5, 201, 1257$   $\mu\text{L/s}$ .

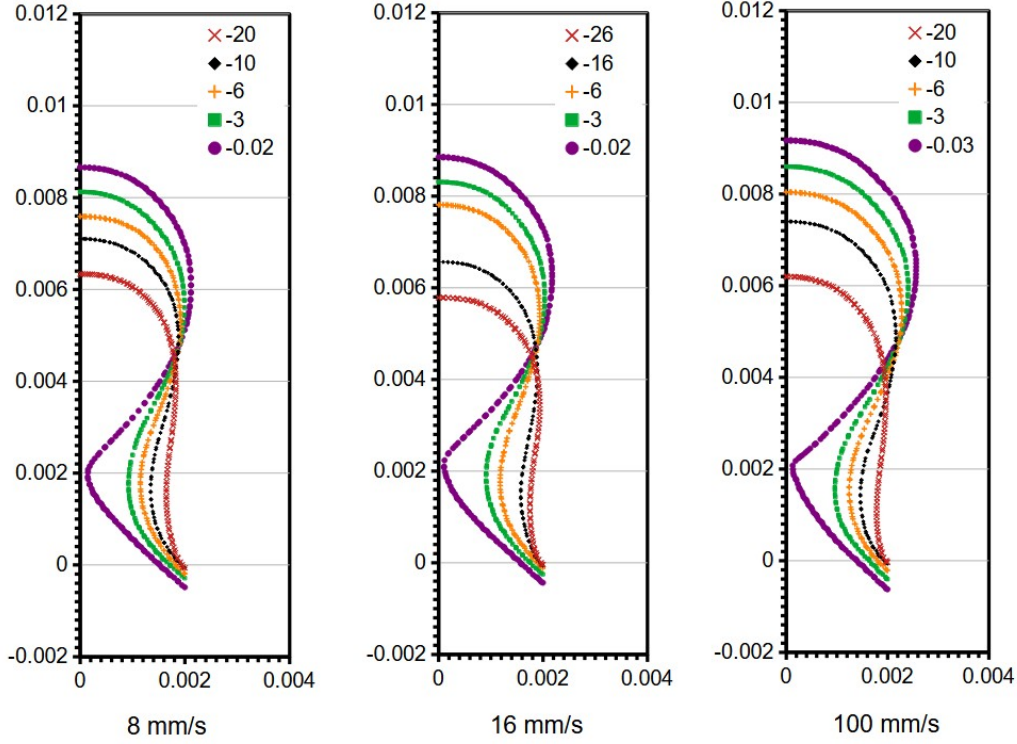


Figure 4. As figure 3 but for bubble growth toward necking pinch-off.

$$V = (\phi_a t_\sigma)Q + (\phi_b V_F) , \quad (7)$$

should be less than the Fritz volume  $V_F$  as observed in table 1. If both  $\phi_a$  and  $\phi_b$  are independent of  $Q$ , (7) suggests a linear relationship between  $V$  and  $Q$  instead of a constant, consistent with the physical expectation.

With the default setting of contact angle  $\theta_0 = 45^\circ$  (with  $\theta_A = 60^\circ$  and  $\theta_R = 30^\circ$ ), figures 3 and 4 also reveal that the three-phase contact line could move along the vertical inner wall of the inlet tube, which has not been recognized in the published literature. The dynamic contact line can reach the deepest location ( $r = 2$  mm,  $z = -0.43$  mm for  $U = 0.016$  m/s) into the inner tube wall as the bubble detachment occurs, while outside the time interval of  $-t_\sigma < t < t_\sigma$  (where  $t_\sigma \sim 11$  ms) the contact line appears to stay pinned at the orifice edge ( $r = 2$  mm,  $z = 0$ ). Such a phenomenon of contact line movement seems to be driven by the capillary effects within the capillary timescale.

Because Oguz and Prosperetti (1993) used a ‘90°-rule’ for contact angle, a case of  $\theta_0 = 90^\circ$  is computed for  $U = 0.016$  m/s ( $Q = 201$   $\mu\text{L/s}$ ). The computed results show  $\Delta T = 292$  ms with  $V = 58.71$   $\text{mm}^3$  and  $d = 4.82$  mm, which are practically not different from the corresponding

values in table 1. However, with  $\theta_0 = 90^\circ$  the contact line is pinned at the orifice edge (referred to as ‘mode A’ bubble formation in Gerlach et al. 2005), in contrast to the case of  $\theta_0 = 45^\circ$  in figures 3 and 4. The bubble surface profiles shown by Oguz and Prosperetti (1993) indeed seem to have pinned contact lines at the thin-wall needle edge. According to the present results, the detached bubble volume at a given gas flow rate does not seem to vary much when the liquid is adequately wetting the orifice wall with the contact angle less than that for contact line pinning at the orifice edge, because the contact diameter  $d_c$  remains the same as  $D$  regardless how the contact line moves on the inlet tube wall.

However, if the contact angle is increased to  $\theta_0 = 120^\circ$  with  $U = 0.016$  m/s ( $Q / Q_{crit} = 0.0533$ ), we would now obtain  $\Delta T = 483$  ms with  $V = 97.11$  mm<sup>3</sup> and  $d = 5.70$  mm, while the contact line could reach as far as  $r \sim 4$  mm along the horizontal surface of  $z = 0$  during the time outside the interval  $(-t_\sigma, t_\sigma)$ . For  $\theta_0 = 105^\circ$ , we then obtain  $\Delta T = 347$  ms with  $V = 69.77$  mm<sup>3</sup> and  $d = 5.11$  mm, also with the contact line moving on the horizontal outside wall of the orifice. Actually, the contact line could move on the horizontal surface when  $\theta_0 > 95^\circ$  (for  $\theta_0 = 95^\circ$ , the contact line appears barely pinned at the orifice edge with the value of  $\Delta T$  being within a few percent of that for  $\theta_0 = 45^\circ, 90^\circ$ ). The situation when the contact line moves on the horizontal outside wall of the orifice during bubble formation is referred to as ‘mode B’ in Gerlach et al. (2005). In mode B the bubble volume was shown to increase with the contact angle almost exponentially from  $\theta_0 \sim 50^\circ$  to  $110^\circ$  (Gerlach et al. 2007) because the time-dependent contact diameter  $d_c$  is always greater than the orifice diameter  $D$ .

For a given geometric setting, there exists a critical contact angle  $\theta_c$  (e.g.,  $\sim 95^\circ$  for  $D = 4$  mm at  $U = 0.016$  m/s) dividing the Mode A and Mode B regimes, namely below  $\theta_c$  the contact line could move along the vertical inner wall of inlet channel whereas above  $\theta_c$  the contact line is moving on the horizontal outside wall of the orifice. The motion of the contact line along the vertical inner wall has little effect on detached bubble size, but the bubble size can be quite sensitive to the contact line motion on the horizontal outside wall of the orifice due to transient variation of the contact diameter. The fact that below a critical contact angle  $\theta_c$  the detached bubble size appears independent of the contact angle was also reported by Manoharan et al. (2021) in their experiments.

### 3.1.2 Case of $D = 2$ mm

For  $D = 2$  mm, the reference values of  $V_F$  and  $d_F$  are 44.83  $\mu$ L and 4.41 mm with  $Q_{crit} = 2115.15$   $\mu$ L/s and  $t_\sigma = 3.78$  ms. To compare with a result of  $d = 4.40$  mm for  $Q \sim 391$   $\mu$ L/s by Oguz and Prosperetti (1993), a case of  $\theta_0 = 90^\circ$  is computed here for  $U = 0.125$  m/s ( $Q = 392.70$   $\mu$ L/s) which yields  $\Delta T = 147$  ms with  $V = 57.73$  mm<sup>3</sup> and  $d = 4.80$  mm. If  $\theta_0$  were reduced to  $80^\circ$ , we would have  $\Delta T = 101$  ms with  $V = 39.66$  mm<sup>3</sup> and  $d = 4.23$  mm. However, with the present model, the contact line would move on the horizontal outside wall of the orifice for  $\theta_0 > 60^\circ$  (at  $\theta_0 = \theta_c \sim 60^\circ$  the contact line appears barely pinned at the orifice edge with computed  $\Delta T = 80$  ms). Given  $\theta_c \sim 95^\circ$  for  $D = 4$  mm, the computed case of  $D = 2$  mm suggests a decreasing trend of  $\theta_{crit}$  with reducing orifice size. As a reference, the value of  $V_B$  from (5) for  $\theta_0 < \theta_c$  would become  $\sim 29.53$  mm<sup>3</sup> for  $D = 2$  mm at low gas flow rates for quasi-static bubble formation.

Table 2 presents the computed results for  $Q \sim 393$  and  $1668 \mu\text{L/s}$  each at  $\theta_0 = 45^\circ$  and  $75^\circ$ , respectively. The former is intended to be compared with a case reported by Oguz and Prosperetti (1993). while the latter with some results of Gerlach et al. (2007) who reported  $\Delta T = 42, 54, 126$  ms for  $\theta_0 = 0^\circ, 70^\circ, 110^\circ$ , respectively at  $Q = 1667 \mu\text{L/s}$  ( $100 \text{ mL/min}$ ) with their numerical simulations using a static contact angle model (i.e., for  $\theta_A = \theta_R = \theta_0$ ).

Table 2. As table 1 but for  $D = 2$  mm with  $V_F = 44.83 \mu\text{L}$ ,  $d_F = 4.41$  mm,  $Q_{crit} = 2115.15 \mu\text{L/s}$ .

$U$ (m/s)	$Q$ ( $\mu\text{L/s}$ )	$\theta_0$ (deg)	$\Delta T$ (ms)	$V$ ( $\text{mm}^3$ )	$d$ (mm)	$Q / Q_{crit}$
0.125	392.70	45	80	31.42	3.91	0.186
		75	93	36.52	4.12	
0.531	1668.18	45	36	60.05	4.86	0.789
		75	47	78.40	5.31	

Apparently, the present results consistently show smaller bubble volume than those reported by both Oguz and Prosperetti (1993) and Gerlach et al. (2007). Although the governing equations for the bubble formation problem are mostly the same, the treatments of the dynamic behavior of the contact line are noticeably different between the present model and those of previous authors. Before resolving the exact causes (which can be extremely difficult due to inaccessible source codes), the differences beyond normally acceptable numerical tolerance may be attributed to the differences in the mathematical representation of the dynamic contact line, for now. Nonetheless, the present results are in qualitative agreement with the previous publications with the same trends for variations of wetting angle and gas flow rate.

To provide a reference for the “quasi-static regime” at a low gas flow rate, a computed case of  $U = 0.05$  m/s ( $Q / Q_{crit} = 0.0743$ ) shows the bubble diameter  $d = 3.81$  mm corresponding to a volume  $V = 28.90 \text{ mm}^3$  for  $\Delta T = 184$  ms with  $\theta_0 = 45^\circ$  (which is practically the same as that up to  $\theta_0 = 75^\circ$ ). Now, the critical contact angle becomes  $\theta_c \sim 75^\circ$  (for the contact line pinned at the orifice edge), indicating an increase of  $\theta_c$  with reducing the gas flow rate. But with  $\theta_0 = 90^\circ$  significant contact line motion on the horizontal outside wall of the orifice occurs, leading to  $d = 4.59$  mm,  $V = 50.74 \text{ mm}^3$  for  $\Delta T = 323$  ms. Actually, the contact line motion on the horizontal outside wall of the orifice becomes obvious at  $\theta_0 = 80^\circ$  with  $\Delta T = 219$  ms,  $V = 34.40 \text{ mm}^3$ , and  $d = 4.04$  mm. Again, the present results for partially wetting liquids with  $\theta_0 < \theta_c$  agree well with the fixed contact line value of  $V_B \sim 29.53 \text{ mm}^3$  from (5) for  $D = 2$  mm.

Further comparison with some computed bubble surface profiles of Gerlach et al. (2007) for  $\theta_0 = 0^\circ, 70^\circ$ , and  $110^\circ$  at  $Q = 1667 \mu\text{L/s}$  and  $t = 0, \Delta T/3, 2 \Delta T/3$  is provided in figure 5 with the present computational results for  $\theta_0 = 45^\circ, 75^\circ$ , and  $105^\circ$  exhibiting similar contact line motion on the horizontal surface (which could occur for  $\theta_0 > 60^\circ$  per present computations). The bubble surface profiles in figure 5 look generally comparable to those of Gerlach et al. (2007).

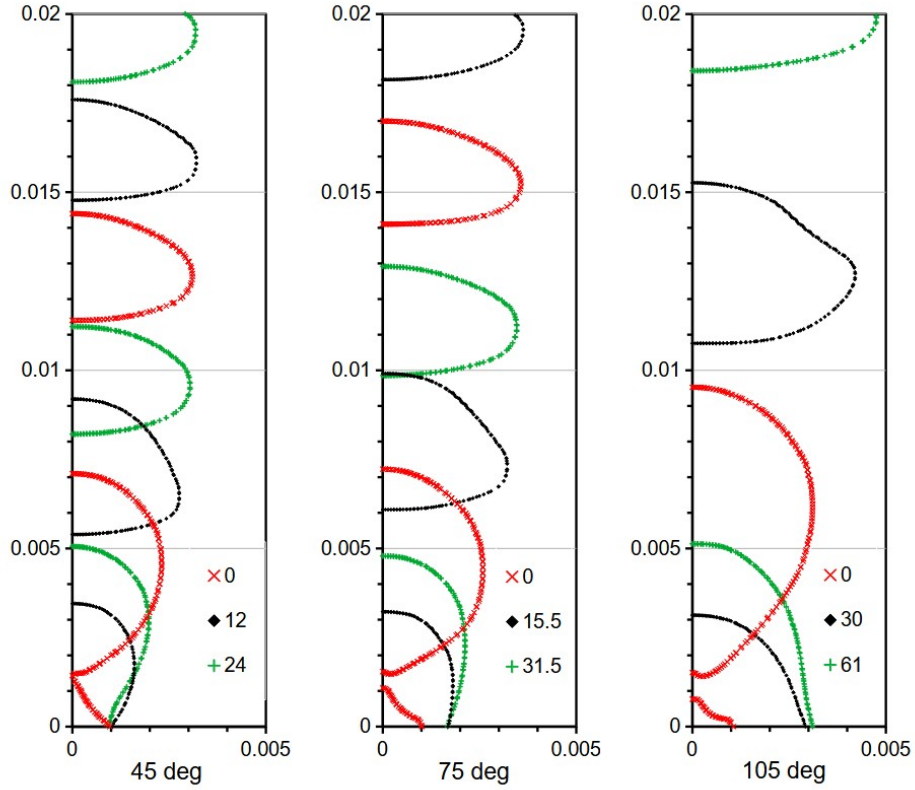


Figure 5. As figure 3 but for  $D = 2$  mm at  $U = 0.531$  m/s corresponding to  $Q = 1668$   $\mu\text{L/s}$  for  $\theta_0 = 45^\circ$ ,  $75^\circ$ ,  $105^\circ$  (with  $\theta_A = \theta_0 + 15^\circ$  and  $\theta_R = \theta_0 - 15^\circ$ ) and  $\Delta T = 36, 47, 91$  ms.

For the record, a fitted line can be obtained as  $V(x) = 44.24x + 24.49 \text{ mm}^3$  with  $R^2 > 0.997$  for  $\theta_0 = 45^\circ$  and  $D = 2$  mm with computed data for  $x = Q / Q_{crit}$  from 0.037 up to 1.04. This is consistent with (7) having  $\phi_a t_\sigma Q_{crit} = 44.24 \text{ mm}^3$  and  $\phi_b V_F = 24.49 \text{ mm}^3$  corresponding to  $\phi_a \sim 5.53$  and  $\phi_b \sim 0.55$ . Unlike that seen in figure 2 for  $D = 4$  mm with pairing bubbles at  $Q / Q_{crit} = 1$ , here for  $D = 2$  mm those detached bubbles remain period-1 when  $Q / Q_{crit} = 1.04$  (with pairing bubbles observed at  $Q / Q_{crit} = 1.485$  as slight movements of the contact line can be noticed on the horizontal outside wall of the orifice, consistent with the decreasing trend of  $\theta_c$  with the gas flow rate  $Q$ .)

### 3.1.3 Case of $D = 1.5$ mm

In a study of the wetting effects on bubble formation, Manoharan et al. (2021) presented experimental results for a list of averaged bubble diameters detached from  $D = 1.5$  mm with different contact angles for water, in the quasi-static regime (for  $Q < 150$   $\mu\text{L/s}$  or  $< 9$  mL/min

such that  $Q/Q_{crit} < 0.09$ ):  $d = 2.75, 2.69, 2.98, 3.78, 3.98, 4.27$  mm with  $\theta_0 = 43^\circ, 52^\circ, 62^\circ, 105^\circ, 120^\circ, 128^\circ$  (in their table 2).

For  $D = 1.5$  mm, we would have  $V_F = 33.63$   $\mu\text{L}$  and  $d_F = 4.00$  mm with  $Q_{crit} = 1664.28$   $\mu\text{L/s}$  and  $t_\sigma = 2.45$  ms. Yet the value of  $d = 3.52$  mm corresponds to  $V_B = 22.90$   $\text{mm}^3$  from (5), in reasonable agreement with the present computational results in table 3 for  $\theta_0 < \theta_c \sim 65^\circ$ . Noteworthy here is that at  $\theta_0 = 70^\circ$  even with noticeable contact line motion on the horizontal outside wall of the orifice, the computed bubble size does not seem to change from that for  $\theta_0 < 65^\circ$  (with  $Q/Q_{crit} = 0.053$  corresponding to  $U = 0.05$  m/s). In this case, the contact line motion on the horizontal outside wall of the orifice occurs only when  $\sim 15$  ms away from the time of meniscus pinch-off, much longer than  $t_\sigma = 2.45$  ms.

Table 3. As table 1 but for  $D = 1.5$  mm with  $V_F = 33.63$   $\mu\text{L}$ ,  $d_F = 4.00$  mm,  $Q_{crit} = 1664.28$   $\mu\text{L/s}$ .

$U$ (m/s)	$Q$ ( $\mu\text{L/s}$ )	$\theta_0$ (deg)	$\Delta T$ (ms)	$V$ ( $\text{mm}^3$ )	$d$ (mm)	$Q/Q_{crit}$
		45	218	19.26	3.32	
		60	214	18.91	3.31	
0.05	88.36	75	283	25.01	3.63	0.053
		90	540	47.71	4.50	
		105	888	78.46	5.31	
		120	884	78.11	5.30	

It is interesting to note that the bubble sizes in table 3 are consistently greater than those corresponding ones shown by Manoharan et al. (2021), unlike other comparisons with previously published data. However, the present results for  $\theta_0 < 75^\circ$  are in good agreement with the value of  $V_B$  according to (5) based on the experiments of Bari and Robinson (2013) for quasi-static bubble formation with fixed contact lines.

### 3.1.4 Case of $D = 1$ mm

Reducing orifice size to  $D = 1$  mm would have  $V_F = 22.42$   $\mu\text{L}$  and  $d_F = 3.50$  mm with  $Q_{crit} = 1187.09$   $\mu\text{L/s}$  and  $t_\sigma = 1.34$  ms, while  $V_B = 16.00$   $\mu\text{L}$  (corresponding to  $d = 3.13$  mm) from (5). Table 4 shows the computed results for  $D = 1$  mm at  $Q/Q_{crit} = 0.033$  and at various  $\theta_0$  with  $\theta_c < 60^\circ$  (at  $\theta_0 = 60^\circ$  the contact line motion on the horizontal outside wall of the orifice is observable although the detached bubble volume does not seem to increase). Noteworthy here is that at  $\theta_0 = 65^\circ$  with substantial contact line movements on the horizontal outside wall of the orifice, the

detached bubble volume remains comparable to that at  $\theta_0 < \theta_c$ . Even up to  $\theta_0 = 70^\circ$  the detached bubble volume remains about the same as  $V_B$  (though larger than that with  $\theta_0 = 65^\circ$  for quasi-static bubble formation based on the present computational model.)

Some experimental results of bubble formation in water for  $D = 1$  mm at  $Q = 48.4$   $\mu\text{L/s}$  ( $U \sim 0.0616$  m/s) with  $\theta_0 = 68^\circ$  were presented by Corchero et al. (2006) with bubbles of  $V \sim 22.4$   $\text{mm}^3$  and  $d \sim 3.5$  mm. This seems quite comparable to the values of  $V_F$  and  $d_F$  at  $\theta_0 \sim 75^\circ$  according to the present results shown in table 4. Such an imperfect quantitative comparison between the computational model and experiment may not be surprising given the intrinsic limitations of macroscopic continuum models for the dynamic contact line (cf. Blake and Ruschak 1997; Chen et al. 2009) as well as difficulties in experimentally measuring the moving contact line behavior. Based on the present computational findings, it is clear that the preferred comparison cases would be those with  $\theta_0 < \theta_c$  where the detached bubble sizes are insensitive to the actual  $\theta_0$  values. The situation of  $\theta_0 < \theta_c$  could also be practically desirable for minimizing the bubble size with improved process consistency. However, model prediction of the value of  $\theta_c$  for contact line pinning is likely to depend on dynamic contact line formulation, and surface properties of the orifice materials.

Table 4. As table 1 but for  $D = 1$  mm with  $V_F = 22.42$   $\mu\text{L}$ ,  $d_F = 3.50$  mm,  $Q_{crit} = 1187.09$   $\mu\text{L/s}$ .

$U$ (m/s)	$Q$ ( $\mu\text{L/s}$ )	$\theta_0$ (deg)	$\Delta T$ (ms)	$V$ ( $\text{mm}^3$ )	$d$ (mm)	$Q / Q_{crit}$
0.05	39.27	45	274	10.76	2.74	0.033
		65	282	11.07	2.77	
		70	419	16.45	3.16	
		75	586	23.01	3.53	

To examine the effect of gas flow rate  $Q$  for  $\theta_0 < \theta_c$  cases at  $\theta_0 = 45^\circ$  with  $Q = 392.7$   $\mu\text{L/s}$  ( $U = 0.5$  m/s,  $Q / Q_{crit} = 0.331$ ),  $Q = 1178.1$   $\mu\text{L/s}$  ( $U = 1.5$  m/s,  $Q / Q_{crit} = 0.992$ ), and  $Q = 1570.8$   $\mu\text{L/s}$  ( $U = 2$  m/s,  $Q / Q_{crit} = 1.323$ ) are also computed here. As consistent with that already being observed, increasing  $Q / Q_{crit}$  to  $> 0.992$  would reduce the value of  $\theta_c$  to  $< 45^\circ$ , because now the contact line motion at  $\theta_0 = 45^\circ$  is noticeable on the horizontal outside wall of the orifice.

Again, the computed data at  $Q / Q_{crit} = 0.033, 0.331, 0.992, 1.323$  for  $\theta_0 = 45^\circ$  can be fitted into a line of  $V$  versus  $x = Q / Q_{crit}$  as  $V(x) = 21.45 x + 9.179$   $\text{mm}^3$  with  $R^2 > 0.995$  in the form of (7) having  $\phi_a \sim 13.52$  and  $\phi_b \sim 0.41$ . Comparing the values of  $\phi_a$  and  $\phi_b$  for the case of  $D = 2$  mm, the differences suggest that  $\phi_a$  and  $\phi_b$  are at least orifice-size dependent. The phenomenon of bubble pairing for an orifice of  $D = 1$  mm with  $\theta_0 = 45^\circ$  does not seem to occur until  $Q / Q_{crit} = 2.32$ , when  $U = 3.5$  m/s with  $\Delta T = 23.6$  ms,  $V = 64.87$   $\text{mm}^3$  and  $d = 4.99$  mm (which is above but not too far from the value from the fitted linear formula  $V(2.32) = 58.85$

mm<sup>3</sup>). It should be noted that the value of  $V$  here is obtained from the neck pinch-off period  $\Delta T$  for individual bubbles before pairing coalescence. Obviously, the value of  $Q / Q_{crit}$  for pairing bubbles increases by reducing the orifice size.

Moreover, Mirsandi et al. (2020) showed experimental as well as computational results for  $D = 1$  mm around  $Q = 21.8$   $\mu\text{L}/\text{min}$  (i.e.,  $363$   $\mu\text{L}/\text{s}$  and  $U \sim 0.462$  m/s) with  $\theta_0 \sim 105^\circ$  and  $\Delta T \sim 351$  ms, apparently corresponding to bubbles of  $V \sim 127$  mm<sup>3</sup> and  $d \sim 6.2$  mm. For comparison, a case of  $U = 0.462$  m/s at  $\theta_0 \sim 105^\circ$  (with  $\theta_A = 120^\circ$  and  $\theta_R = 90^\circ$ ) is computed here to yield bubbles of  $V = 87.08$  mm<sup>3</sup> and  $d = 5.50$  mm, significantly larger than that with  $\theta_0 = 45^\circ$  (i.e., having  $V(0.306) \sim 15.5$  mm<sup>3</sup>) but not quite as large as that of Mirsandi et al. If the value of  $D$  were increased to 2 mm and 4 mm with all other parameters kept the same (for  $Q \sim 363$   $\mu\text{L}/\text{s}$ ), the resulting  $d$  would respectively become 5.63 and 5.57 mm, not much different from  $d = 5.50$  mm with  $D = 1$  mm. Then, for non-wetting liquids to the orifice wall, the bubble size may not decrease by reducing the orifice size at a given gas flow rate.

### 3.2 Air bubbles in an aqueous-glycerol solution

For air bubbles forming from an orifice of  $D = 1.7$  mm in an aqueous-glycerol solution with  $\rho = 1223.8$  kg m<sup>-3</sup>,  $\sigma = 0.066$  kg s<sup>-2</sup>, and  $\mu = 0.126$  kg m<sup>-1</sup> s<sup>-1</sup> (Helsby and Tuson 1955; Ohta et al. 2011), the values of  $V_F$  and  $d_F$  become 29.36  $\mu\text{L}$  and 3.83 mm. In this case, the Ohnesorge number from (3) would take a value of  $Oh = 0.2895$ , considerably larger than  $2.313 \times 10^{-3}$  for the air-water system as an exemplifying case for the effect of increasing viscosity by two orders of magnitude.

Table 5. As table 1 but for  $D = 1.7$  mm,  $\rho = 1223.8$  kg m<sup>-3</sup>,  $\sigma = 0.066$  kg s<sup>-2</sup>, and  $\mu = 0.126$  kg m<sup>-1</sup> s<sup>-1</sup> with  $V_F = 29.36$   $\mu\text{L}$ ,  $d_F = 3.83$  mm,  $Q_{crit} = 1486.40$   $\mu\text{L}/\text{s}$ .

$U$ (m/s)	$Q$ ( $\mu\text{L}/\text{s}$ )	$\theta_0$ (deg)	$\Delta T$ (ms)	$V$ (mm <sup>3</sup> )	$d$ (mm)	$Q / Q_{crit}$
0.088	199.74	45	140.5	28.06	3.77	0.134
		75	171	34.16	4.03	
0.441	1000.98	45	60.5	60.56	4.87	0.673
		75	72	72.07	5.16	
0.881	1999.69	45	48.2	96.39	5.69	1.345
		75	56.0	111.98	5.98	

Table 5 shows the present model results for  $U = 0.088, 0.441, 0.881$  m/s at  $\theta_0 = 45^\circ$  and  $75^\circ$ , for comparing with a set of computational results reported by Ohta et al. (2011), i.e.,  $d =$



4.22, 4.89, 5.49 mm, and corresponding experimental results of Helsby and Tuson (1955) as  $d = 4.06, 4.99, 5.72$  mm. Since both Helsby and Tuson (1955) and Ohta et al. (2011) were considering bubble detaching from a thin-wall needle rather than an orifice on a plane surface, their results should be described reasonably by the present model for cases of  $\theta_0 = 45^\circ$  with contact diameter remaining constant. For reference, the cases of  $\theta_0 = 75^\circ$  are also presented here. Indeed, the present computations for  $\theta_0 = 45^\circ$  yield results in good agreement with Helsby as well as Tuson (1955) and Ohta et al. (2011), although for the case of  $U = 0.088$  m/s using  $\theta_0 = 75^\circ$  seems to offer even better agreement. Interestingly, the present values of  $V = 28.06$  mm<sup>3</sup> and  $d = 3.77$  mm at  $Q / Q_{crit} = 0.134$  are rather closer to  $V_F = 29.36$   $\mu$ L and  $d_F = 3.83$  mm than those of Helsby & Tuson (1955) and Ohta et al. (2011). That increased viscosity improves the accuracy of the Fritz bubble size for quasi-static cases might be explained by the nature of viscosity to hamper the capillary-force-driven dynamics during the neck pinch-off process.

Another observation from the computed results with  $Oh = 0.2895$  indicates that in a liquid of higher viscosity, the detached bubbles exhibit little surface deformations from the spherical shape, as expected from viscous suppression of surface-tension-driven oscillations. Here the computed bubble rising velocity is in the range of 0.1 to 0.2 m/s, comparable to those by Ohta et al. (2011). Thus, with  $\rho = 1223.8$  kg m<sup>3</sup>,  $\sigma = 0.066$  kg s<sup>-2</sup>, and  $\mu = 0.126$  kg m<sup>-1</sup> s<sup>-1</sup> for a bubble of  $d = 4$  mm and rising velocity of 0.2 m/s, the estimated rising bubble Reynolds number would be  $Re \sim 9.7$  and Weber number  $We \sim 3.7$  which would not cause substantial steady-state bubble surface deformation (cf. Feng 2007), either.

### 3.3 Air bubbles in a liquid of lower surface tension

So far the computed cases are relevant to air bubbles in aqueous liquids with surface tension around  $\sigma \sim 0.07$  kg s<sup>-2</sup>, because most available experimental data are obtained with the air-water systems for laboratory convenience. Here, the case of reduced surface tension computed for  $D = 1$  mm and  $\theta_0 = 45^\circ$  at  $U = 0.05$  m/s with  $\sigma = 0.035$  kg s<sup>-2</sup> (as representative to many non-aqueous solvents) and everything else the same as that for the air-water systems. This is a purely computational benchmark study against the corresponding case for  $\sigma = 0.07$  kg s<sup>-2</sup> with  $\Delta T = 274$  ms and  $V = 10.76$  mm<sup>3</sup> as in table 4. The resulting  $\Delta T$  becomes 152.5 ms with  $V = 5.99$  mm<sup>3</sup> which is about 10% greater than  $0.5 \times 10.76 = 5.38$  mm<sup>3</sup> but slightly closer than the air-water case to that estimated by (1) for the quasi-static situation. Again, the Fritz formulas in (1), based on a static force balance between surface tension and buoyancy, may only offer values for rough estimates rather than accurate predictions in specific applications, because other effects could be more influential, especially with reduced surface tension.

## 4 Concluding Remarks

The OpenFOAM<sup>®</sup> VOF computational model presented here can yield numerical results in general qualitative agreement with most of those reported by previous authors, which in some sense verifies the model's validity. For example, the results show that the detached bubble size tends to increase with the gas flow rate, orifice size, surface tension, liquid contact angle, etc.

There exists a critical gas flow rate above which detached bubbles will combine via coalescence and exhibit the bubble pairing phenomenon. The detached bubble size seems insensitive to the liquid contact angle when it is smaller than a critical value (referred to as Mode A by Gerlach et al. 2005), but can increase substantially at larger contact angles which results in the contact line movement on the horizontal outside wall of the orifice (Mode B per Gerlach et al. 2005). To avoid being deeply involved in the complexities of the Mode B bubble formation process, the present work mainly focuses on analyzing the Mode A cases with a few Mode B cases computed for brief demonstrative purposes. Operating with Mode A can be accomplished by using orifice materials that allow adequate liquid wetting, and is desirable for the convenience of process control and minimizing the bubble size.

On the other hand, the present computational study also reveals some details not yet recognized by previous authors. The majority of publications in the literature tend to claim that the detached bubble volume would become about the same as the Fritz value  $V_F$  in (1) irrespective of gas flow rate when  $Q / Q_{crit} < 1$ , whereas the present study shows a linear relationship between  $V$  and  $Q$  with the slope increasing with orifice size (cf. table 6 based on results for  $\theta_0 = 45^\circ$  when the liquid 'wets' the orifice walls).

Table 6. Fitted values of  $a$  and  $b$  in the linear relationship of  $V$  versus  $x = Q / Q_{crit}$  as  $V(x) = ax + b$  for  $D = 1, 2, 4$  mm with  $x$  up to 1 (or not too far above 1), based on results for  $\theta_0 = 45^\circ$ .

$D$ (mm)	$Q_{crit}$ ( $\mu\text{L/s}$ )	$a$ ( $\text{mm}^3$ )	$b$ ( $\text{mm}^3$ )	$V_F$ ( $\text{mm}^3$ )
1	1187.09	21.446	9.179	22.42
2	2115.15	44.239	24.493	44.83
4	3768.77	103.84	52.710	89.67

In terms of coefficients  $\phi_a$  and  $\phi_b$  in (7), we would have  $\phi_a = 13.52, 5.53, 2.58$  and  $\phi_b = 0.41, 0.55, 0.59$ , respectively for  $D = 1, 2, 4$  mm. To account for the orifice-size dependence, both  $\phi_a$  and  $\phi_b$  may be approximated as functions of  $D/L_\sigma$  such that

$$\phi_a \simeq 0.415 \left( \frac{L_\sigma}{D} \right)^{6/5} \quad \text{and} \quad \phi_b \simeq 0.54 \left( \frac{D}{L_\sigma} \right)^{1/4}, \quad (8)$$

where  $(D/L_\sigma)$  turns out the same as the square root of the Bond number  $Bo = (\rho g D^2 / \sigma)$  for measuring the relative importance of gravitational forces compared to the capillary forces. The trends of  $\phi_a$  decreasing while  $\phi_b$  increasing with  $(D/L_\sigma)$  or  $Bo$  indicated by (8) would mean that reducing the orifice size  $D$  enhances the relative effects of capillary-force-driven dynamics on detached bubble volume, in terms of the physical meaning of (7). According to present model findings, the effects of capillary dynamics tend to reduce the bubble size from that of the Fritz value. Such computed bubble volumes for  $Q / Q_{crit} \ll 1$ , generally smaller than  $V_F$ , seem in good

agreement with the experiments of Bari & Robinson (2013) for quasi-static bubble growth with fixed contact lines. If further independently confirmed, this finding could be good news because smaller bubbles with a given orifice size are often more desirable for heat and mass transfer applications.

However, having smaller bubbles also requires using relatively lower gas flow rates (e.g., with  $Q / Q_{crit} < 0.1$ ), which would compromise the bubble throughput per orifice—a significant factor to consider in process development. Moreover, according to the present findings, the critical contact angle  $\theta_c$  dividing Mode A and Mode B regimes decreases with reducing the orifice size and with increasing the gas flow rate. This would make reducing orifice size for generating smaller bubbles more challenging and practically difficult with constant gas flow, especially for  $D < 1$  mm. The experiments of Mohseni et al. (2020) with laser-machined sub-millimeter orifices on stainless steel plates in water with measured  $\theta_0 \sim 75^\circ$  demonstrated that bubbles detached from a  $D = 0.4$  mm orifice could have  $V \sim 21, 27, 32$  mm<sup>3</sup> at  $Q = 167, 500, 833$   $\mu\text{L/s}$  (with  $Q_{crit} \sim 553$   $\mu\text{L/s}$ ), generally larger than that from a  $D = 1$  mm orifice as a consequence of much higher gas flow rate than  $Q = 39.27$   $\mu\text{L/s}$  (cf. table 4).

Besides gaining a further understanding of the complex bubble formation behavior, using an open-source CFD software for the present study provides a valuable merit: it is accessible to everyone who wants to examine and modify the source code. It could open up new opportunities for future investigation of effects due to various numerical algorithms in resolving differences in published model results. Multiple researchers are enabled to conveniently compare notes and collaborate efforts. In this regard, the present results could offer valuable comparison benchmarks for future model refinement and development.

## Statements and Declarations

**Competing interests** The author has no competing interests to declare.

## References

- Bari S D, Robinson A J (2013) Experimental study of gas injected bubble growth from submerged orifices. *Experimental Thermal and Fluid Science* 44: 124-137
- Blake T D, Ruschak K J (1997) Wetting: Static and dynamic contact lines. In *Liquid Film Coating—Scientific Principles and Their Technological Implications*. Ed. S F Kistler, P M Schweizer. Chapman & Hall, pp 62-97
- Buwa V V, Gerlach D, Durst F, Schlucker E (2007) Numerical simulations of bubble formation on submerged orifices: period-1 and period-2 bubbling regimes. *Chem. Eng. Sci.* 62: 7119-7132
- Chen Y, Mertz R, Kulenovic R (2009) Numerical simulation of bubble formulation on orifice plates with a moving contact line. *Int. J. Multiphase Flow* 35: 66-77

- Christodoulou KN, Scriven LE (1992) Discretization of free surface flows and other moving boundary problems. *J. Comput. Phys.* 99: 39-55
- Clift R, Grace J R, Weber M E (1978) *Bubbles, Drops, and Particles*. Academic Press Inc., New York
- Corchero G, Medina A, Higuera FJ (2006) Effect of wetting conditions and flow rate on bubble formation at orifices submerged in water. *Colloids and Surfaces A: Physicochem. Eng. Aspects* 290: 41-49
- Das A K, Das P K, Saha P (2011) Formation of bubbles at submerged orifices—experimental investigation and theoretical prediction. *Exp. Therm. Fluid Sci.* 35: 618-627
- Feng JQ (2007) A spherical-cap bubble moving at terminal velocity in a viscous liquid. *J. Fluid Mech.* 579: 347-371
- Feng JQ (2017) A computational study of high-speed microdroplet impact onto a smooth solid surface. *J. Appl. Fluid Mech.* 10(1): 243-256
- Fritz W (1935) Berechnung des maximale volume dampfblasen (Calculation of maximum volume vapor bubbles). *Phys. Z.* 36: 379-384
- Gaddis E S, Vogelpohl A (1986) Bubble formation in quiescent liquids under constant flow conditions. *Chem. Eng. Sci.* 41(1): 97-105
- Gamet L, Scala M, Roenby J, Scheufler H, Pierson J-L (2020) Validation of volume-of-fluid OpenFOAM® isoAdvector solvers using single bubble benchmarks. *Comput. Fluids* 213: 104722
- Gerlach D, Biswas G, Durst F, Kolobraric V (2005) Quasi-static bubble formation on submerged orifices. *Int. J. Heat Mass Transfer.* 48: 425-438
- Gerlach D, Alleborn N, Buwa V, Durst F (2007) Numerical simulation of periodic bubble formation at a submerged orifice with constant gas flow rate. *Chem. Eng. Sci.* 62: 2109-2125
- Harkins W D, Brown F E (1919) The determination of surface tension (free surface energy) and the weight of falling drops: The surface tension of water and benzene by the capillary height method. *Journal of the American Chemical Society* 41: 499-525
- Higuera FJ (2005) Injection and coalescence of bubbles in a very viscous liquid. *J. Fluid Mech.* 530: 369-378
- Hirt CW, Nichols BD (1981) Volume of fluid (VOF) method for the dynamics of free boundaries. *J. Comput. Phys.* 39(1): 201-225
- Jamialahmadi M, Zehtaban M R, Muller-Steinhagen H, Sarrafi A, Smith J M (2001) Study of bubble formation under constant flow conditions. *Chem. Eng. Res. Des.* 79: 523-532

Kistler SF, Scriven LE (1983) Coating flows. In Computational Analysis of Polymer Processing, Ed. JRA Pearson, SM Richardson, Springer, pp 243-299

Krishna R, Urseanu MI, van Baten JM, Ellenberger J (1999) Rise velocity of a swarm of large gas bubbles in liquids. *Chem. Eng. Sci.* 54(2): 171-183

Kulkarni A A, Joshi J B (2005) Bubble formation and bubble rise velocity in gas-liquid systems: a review. *Ind. Eng. Chem. Res.* 44: 5873-5931

Kumar R, Kuloor N R (1970) The formation of bubbles and drops. *Adv. Chem. Engng.* 8: 256-368

Longuet-Higgins MS, Kerman BR, Lunde K (1991) The release of air bubbles from an underwater nozzle. *J. Fluid Mech.* 230: 365-390

Matkovic M, Koncar B (2012) Bubble departure diameter prediction uncertainty. *Science and Technology of Nuclear Installations*

Manoharan S, Manglik R M, Jog M A (2021) Wetting and capillarity effects on bubble formation from orifice plates submerged in pools of water. *Transactions of the ASME Journal of Heat Transfer* 143: 101602

Mirsandi H, Smit W J, Kong G, Baltussen M W, Peters E A J F, Kuipers J A M (2020) Influence of wetting conditions on bubble formation from a submerged orifice. *Experiments in Fluids* 61: 83

Mohseni E, Kalayathine J J, Reinecke S F, Hampel U (2020) Dynamics of bubble formation at micro-orifices under constant gas flow conditions. *Int J Multiphase Flow* 132: 103407

Mulbah C, Kang C, Mao N, Zhang W, Shaikh A R, Teng S. (2022) A review of VOF methods for simulating bubble dynamics. *Progress in Nuclear Energy* 154: 104478

Nichita BA, Zun I, Thome JR (2010) A level set method coupled with a volume of fluid method for modeling of gas-liquid interface in bubbly flow. *J. Fluids Eng.* 132(8): 081302

Oguz H N, Prosperetti A (1993) Dynamics of bubble growth and detachment from a needle. *J. Fluid Mech.* 257: 111-145

Ohta M, Kikuchi D, Yoshida Y, Sussman M (2011) Robust numerical analysis of the dynamic bubble formation process in a viscous liquid. *Int. J. Multiphase Flow* 37: 1059-1071

Ponter A B, Surati A I (1997) Bubble emissions from submerged orifices—a critical review. *Chem. Eng. Technol.* 20(2): 85-89

Roenby J, Bredmose H, Jasak H (2016) A computational method for sharp interface advection. *Royal Society Open Science* 3: 160405

Sethian JA (1999) *Level Set Methods and Fast Marching Methods: Evolving Interfaces in Computational Geometry, Fluid Mechanics, Computer Vision, and Materials Science*. Cambridge University Press

Simmons J A, Sprittles J E, Shikhmursaev Y D (2015) The formation of a bubble from a submerged orifice. *Euro. J. Mech. B/Fluids* 53: 24-36

Sudepta Vaishnavi GNV, Ramarajan J, Jayavel S (2023) Numerical studies of bubble formation dynamics in gas-liquid interaction using volume of fluid (VOF) method. *Thermal Sci. Eng. Prog.* 39(1): 101718

Sussman M, Fatemi E, Smereka P, Osher S (1998) An improved level set method for incompressible two-phase flows. *Comput. Fluids* 27(5-6): 663-680

Sussman M, Puckett EG (2000) A coupled level set and volume-of-fluid method for computing 3D and axisymmetric incompressible two-phase flows. *J. Comput. Phys.* 162: 301-337

Tufaile A, Sartorelli J C (2000) Chaotic behavior in bubble formation dynamics. *Physica A: Statistical Mechanics and Its Applications* 275(3-4): 336-346

Van Krevelen D, Hoftijzer P (1950) Studies of gas-bubble formation: calculation of interfacial area in bubble contractors. *Chem. Eng. Prog.* 46: 29-35

Wong H, Rumshitzki D, Maldaralli C (1998) Theory and experiment on the low-Reynolds number expansion and contraction of a bubble pinned at a submerged tube tip. *J. Fluid Mech.* 356: 93-124